J|A|C|S
ARTICLES
Published on Web 12/17/2005

Self-organization of Rotaxane Thin Films into Spatially Correlated Nanostructures: Morphological and Structural Aspects

Jean-François Moulin,[†] Jean Crispin Kengne,[†] Rajendra Kshirsagar,[†] Massimilliano Cavallini,[†] Fabio Biscarini,*[,†] Salvador León,[‡,§] Francesco Zerbetto,*[,‡] Giovanni Bottari,[#] and David A. Leigh*[,#]

Contribution from the CNR-ISMN-"Nanotechnology of Multifunctional Materials" Research Division, Via P. Gobetti 101, I-40129 Bologna, Italy, Dipartimento di Chimica "G. Ciamician", Università di Bologna, V. F. Selmi 2, I-40126 Bologna, Italy, and School of Chemistry, University of Edinburgh, The King's Buildings, West Mains Road, Edinburgh EH9 3JJ, U.K.

Received July 21, 2005; E-mail: f.biscarini@bo.ismn.cnr.it; francesco.zerbetto@unibo.it; David.Leigh@ed.ac.uk

Abstract: The self-organization of rotaxane thin films into spatially correlated nanostructures is shown to occur upon a thermal stimulus. The mechanism of formation of nanostructures and their organization has been investigated using atomic force microscopy, bright field transmission electron microscopy, selected area electron diffraction, and molecular mechanics simulations. The evolution of the nanostructures follows a complex pathway, where a rotaxane thin film first dewets from the substrate to form nanosized droplets. Droplets coalesce by ripening, generating spatially correlated motifs. In a later stage, the larger droplets change shape, nucleate, and coalesce to yield crystallites that grow into larger crystals by incorporating the surrounding droplets. The results show the following: (i) the nanostructures represent a metastable state of a crystallization process; (ii) spatial correlations emerge during ripening, but they are destroyed as stable nuclei are formed and crystallization proceeds to completion; iii) crystallization, either on graphite or amorphous carbon films, leads to a precise basal plane, viz. (010), which has minimum surface energy. The inherent degrees of freedom permitted in the rotaxane architecture favors the re-organization and nucleation of the film in the solid state. Low-energy trajectories leading to crystallites with stable surfaces and minimum energy contact plane are found to occur via concerted, small amplitude, internal motions without disruption of packing and intermolecular contacts.

Introduction

Molecular systems that respond to an external stimulus (electrical, chemical, optical, mechanical, or environmental) and modify their geometry accordingly are potentially interesting as nano actuators,[1] building blocks for mechanical molecular machines,[1] and potential memories and sensors.[1] Rotaxanes[2] form a class of molecular architectures with adaptive functionality.[1] Several examples of controllable or triggered motions of the macrocycle with respect to the thread have been reported, resulting in changes to properties such as conductivity,[3] circular dichroism,[4] and fluorescence.[5] These results suggested that new paradigms for switching, information storage, sensing, adaptive surface behavior, and smart coatings could be developed based on rotaxane architectures. However, the degree to which such effects, which have mostly been observed in solution, can be transferred to the condensed phase is not yet clear,[6] especially with regard to the technologically relevant medium of thin films. Nor, indeed, is it clear as to how the stimulus/response can be most effectively controlled.

There have been many studies on the triggered response of rotaxane thin films.[7] The experimental results on electrical switching of a rotaxane system developed by Stoddart and Heath have raised several questions with respect to the intervening

[†] CNR-ISMN.
[‡] Università di Bologna.
[#] University of Edinburgh.
[§] Present address: Department of Chemical Engineering, ETSII/UPM, Jose Gutierrez Abascal, 2, 28006 Madrid, Spain.

(1) (a) Balzani, V.; Credi, A.; Raymo, F. M.; Stoddart, J. F. *Angew. Chem., Int. Ed.* **2000,** *39*, 3348−3391. (b) Balzani, V.; Venturi, M.; Credi, A. *Molecular Devices and Machines − A Journey into the Nanoworld*; Wiley-VCH: Weinheim, 2003. (c) Flood, A. H.; Ramirez, R. J. A.; Deng, W.-Q.; Muller, R. P.; Goddard, W. A.; Stoddart, J. F. *Aust. J. Chem.* **2004**, *57*, 301−322. (d) Kay, E. R.; Leigh, D. A. In *Synthetic Molecular Machines in Functional Artificial Receptors*; Schrader, T., Hamilton, A. D., Eds.; Wiley-VCH: Weinheim, Germany, 2005.

(2) *Molecular Catenanes, Rotaxanes and Knots*: *A Journey Through the World of Molecular Topology*; Sauvage, J.-P., Dietrich-Buchecker, C., Eds.; Wiley-VCH: Germany, 1999.

(3) Collier, C. P.; Wong, E. W.; Belohradsky M.; Raymo, F. M.; Stoddart, J. F.; Kuekes, P. J.; Williams, R. S.; Heath, J. R. *Science* **1999**, *285*, 391−394.

(4) Bottari, G.; Leigh, D. A.; Pérez, E. M. *J. Am. Chem. Soc.* **2003**, *125*, 13360−13361.

(5) (a) Perez, E. M.; Dryden, D. T. F.; Leigh, D. A.; Teobaldi, G.; Zerbetto, F. *J. Am. Chem. Soc.* **2004**, *126*, 12210−12211. (b) Wang, Q.-C.; Qu, D.-H.; Ren, J.; Chen, K.; Tian, H. *Angew. Chem., Int. Ed.* **2004**, *43*, 2661−2665. (c) Qu, D.-H.; Wang, Q.-C.; Ren, J.; Tian, H. *Org. Lett.* **2004**, *6*, 2085−2088. (d) Leigh, D. A. et al. *Angew. Chem., Int. Ed.* **2005**, *44*, 3062−3067.

(6) (a) Flood, A. H.; Peters, A. J.; Vignon, S. A.; Steuerman, D. W.; Tseng, H.-R.; Kang, S.; Heath, J. R.; Stoddart, J. F. *Chem. Eur. J.* **2004**, *10*, 6558−6564. (b) Steuerman, D. W.; Tseng, H.-R.; Peters, A. J.; Flood, A. H.; Jeppesen, J. O.; Nielsen, K. A.; Stoddart, J. F.; Heath, J. R. *Angew. Chem., Int. Ed.* **2004**, *43*, 6486−6491.

 10.1021/ja054886o CCC: $33.50

mechanism, whether it occurs at the single-molecule level[8] or it is due to a local re-organization.[9] Our analysis of the energetics of a different rotaxane system in the solid state suggested that the mobility of the macrocycle with respect to the thread would be enhanced if the hydrogen-bonding ability of the macrocycle was saturated by interactions with the thread rather than by intermolecular interactions.[10] This assertion was supported by atomic force microscopy (AFM) indentation of microcrystals, which demonstrated the larger plasticity of the rotaxane crystals with respect to crystals of either the thread or the macrocycle. We recently reported a remarkable phenomenon whereby a local mechanical perturbation applied with an AFM operated at a precise load force on a region of a rotaxane thin film transforms it into arrays of regularly spaced nanostructures (dots).[11] This self-organization occurs collectively as the perturbation is applied. The phenomenon reminds one of spinodal dewetting[12] since the characteristic length scale is controlled by the film thickness while it does not depend on the details of the perturbation parameters. However, the origin of the nanostructures and spatial correlations was unclear, as was whether internal motions of rotaxanes in the solid state are relevant to the phenomenon. Establishing the relationships between intramolecular motions and multiple scale organization is important to understand the relevant processes of crystallization and phase transformation in polymorphic systems and to provide guidelines for crystal engineering and screening/design of complex molecular materials.[13,14] It allows us to set the basis for further developing functional arrays of rotaxane nanostructures that may act, for instance, as memory elements or sensing elements of an external force.

In this paper, we address the question of the nature of the nanostructures, the mechanism by which spatial correlations emerge and propagate across length scales and to which extent the rotaxane architecture has a specific role in this self-organization in the solid state. We investigate the transformation of thin films of rotaxane **1**[15] (Figure 1) cast on highly oriented pyrolitic graphite, as in ref 11. In the present experiment, the transformation of the thin film is induced by heating the samples at 90 °C (below the melting temperature of **1**, viz. 345 °C). The evolution vs time of annealing is studied by atomic force microscopy (AFM), bright field transmission electron microscopy (TEM), and selected area electron diffraction (SAED).[16]

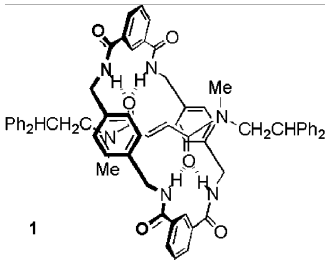

Figure 1. Rotaxane **1** used in this study.

This paper is organized as follows: In the section Results, we describe the morphological and structural evolution of the film into nanostructures and crystals and present the results of molecular mechanics simulations of rotaxane crystallites on the energetics of interconversion from a variety of surfaces to the minimum energy ones; in the section Discussion, we discuss the experimental data in view of the results of the simulations; finally, we draw the Conclusions. The details of the experiments and simulations are reported as Supporting Information.

Results

Thermal Annealing. Figure 2 shows the evolution of a thin film of rotaxane **1**[15] upon heating the sample at 363 K. The sequence of images shows the occurrence of a three-step transformation: (i) the continuous film dewets into an ensemble of hemispherically capped droplets;[17] (ii) droplet size grows in time by ripening[17d,18] and a characteristic length scale emerges as outcome of spatial correlations;[19] (iii) at a later stage, some droplets transform into crystallites which then grow by depleting droplets from the surrounding region. At this later stage, there is no longer a characteristic length scale. Thus, the crystallization wipes out the spatial correlations established earlier.

The spatial correlations are described by means of the height−height correlation function, $g(r) = \langle (h(r) - h(0))^2 \rangle$.[20] Here, $h(r)$ is the topography height for the radial distance r, and the average is performed on the azimuthal coordinate.[21] In Figure 3, $g(r)$ is plotted vs r for the image sequence in Figure 2. The curves at earlier times exhibit a first local maximum at nonzero length scales, and other maxima, damped in intensity, are observed at integer multiple length scales. The position of the first maximum defines the characteristic length scale, viz. correlation length, ξ, whose evolution vs annealing time is shown in the inset.

(7) (a) Katz, E.; Lioubashevsky, O.; Willner, I. *J. Am. Chem. Soc.* **2004,** *126*, 15520−15532. (b) Long, B.; Nikitin, K.; Fitzmaurice, D. *J. Am. Chem. Soc.* **2003,** *125*, 15490−15498. (c) Katz, E.; Sheeney Haj, I.; Willner, I. *Angew. Chem., Int. Ed.* **2004**, *43*, 3292−3300. (d) Huang, T. J. et al. *Nano Lett.* **2004,** *4*, 2065−2071. (e) Tseng, H.-R.; Wu, D.; Fang, N. X.; Zhang, X.; Stoddart, J. F. *ChemPhysChem* **2004**, *5*, 111−116. (f) Jang, S. S. et al. *J. Am. Chem. Soc.* **2005**, *127*, 1563−1575. (g) Hernandez, R.; Tseng, H.-R.; Wong, J. W.; Stoddart, J. F.; Zink, J. I. *J. Am. Chem. Soc.* **2004**, *126*, 3370−3371. (h) Liu, Y. et al. *J. Am. Chem. Soc.* **2005**, *127*, 9745−9759.
(8) Flood, A. H.; Stoddart, J. F.; Steuerman, D. W.; Heath, J. R. *Science* **2004**, *306*, 2055−2056.
(9) Feng, M.; Guo, X.; Lin, X.; He, X.; Ji, X.; Du, W.; Zhang, D.; Zhu, D.; Gao, H. *J. Am. Chem. Soc.* **2005**, *127*, 15338−15339.
(10) Biscarini, F.; Cavallini, M.; Leigh, D. A.; Leon, S.; Teat, S. J.; Wong, J. K. Y.; Zerbetto, F. *J. Am. Chem. Soc.* **2002**, *124*, 225−233.
(11) Cavallini, M.; Biscarini, F.; Leon, S.; Zerbetto, F.; Bottari G.; Leigh, D. A. *Science* **2003**, *299*, 531−531.
(12) (a) Sferrazza, M.; Heppenstall-Butler, M.; Cubitt, R.; Bucknall, D.; Webster, J.; Jones, R. A. L. *Phys. Rev. Lett.* **1998**, *81*, 5173−5176. (b) Herminghaus, S.; Jacobs, K.; Mecke, K.; Bischof, J.; Fery, A.; Ibn-Elhaj, M.; Schlagowski, S. *Science* **1998**, *282*, 916−919. (c) Suh, K. Y.; Lee, H. H. *Phys. Rev. Lett.* **2001**, 87, 135502. (d) Kargupta, K.; Sharma, A. *J. Chem. Phys.* **2002**, *116*, 3042−3051. (e) Seemann, R.; Herminghaus, S.; Jacobs, K. *J. Phys.: Condens. Matter* **2001**, *13*, 4925−4938. (f) Seemann, R.; Herminghaus, S.; Jacobs, K. *Phys. Rev. Lett.* **2001**, 86, 5534−5537.
(13) Braga, D.; Polito, M.; Grepioni, F. *Cryst. Growth Des*. **2004**, *4*, 769−774.
(14) Amabilino, D. B.; Stoddart, J. F. *Chem. Rev.* **1995**, *95*, 2725−2828.
(15) Gatti, F. G.; Leigh, D. A.; Nepogodiev, S. A.; Slawin, A. M. Z.; Teat, S. J.; Wong, J. K. Y. *J. Am. Chem.* Soc. **2001**, *123*, 5983−5989.
(16) Bendersky, L. A.; Gayle, F. W. *J. Res. Natl. Inst. Stand. Technol.* **2001**, *106*, 997−1012.
(17) (a) Reiter, G. *Phys. Rev. Lett.* **1992**, *68*, 75−78. (b) Reiter, G.; Sharma, A. *Phys. Rev. Lett.* **2001**, *87*, 166103. (c) Sehgal, A.; Ferreiro, V.; Douglas, J. F.; Amis, E. J.; Karim, A. *Langmuir* **2002**, *18*, 7041−7048. (d) Reiter, G.; Khanna, R.; Sharma, A. *J. Phys. Condens. Matter* **2003**, *15*, S331−S336.
(18) (a) Zinke-Allmang, M.; Feldman, L. C.; Grabow, M. H. *Surf. Sci. Rep.* **1992**, *16*, 377−463. (b) Carlow, G. R.; Zinke-Allmang, M. *Phys. Rev. Lett.* **1997**, *78*, 4601−4604. (c) Sharma, A.; Khanna, R. *J. Chem. Phys.* **1999**, *110*, 4929−4936. (d) Singh, J.; Sharma, A. *J. Adhes. Sci. Technol.* **2000**, *14*, 145−166.
(19) Brinkmann, M.; Graff, S.; Biscarini, F. *Phys. Rev. B* **2002**, *66*, 165430.
(20) Zhao, Y. P.; Wang, G.-C.; Lu, T.-M In *Experimental Methods in the Physical Sciences;* Celotta, R., Lucatorto, T., Eds.; Academic Press: San Diego, 2001; Vol. 37.
(21) Brinkmann, M.; Biscarini, F.; Taliani, C.; Aiello, I.; Ghedini, M. *Phys. Rev. B* **2000**, *61*, R16339−R16342.

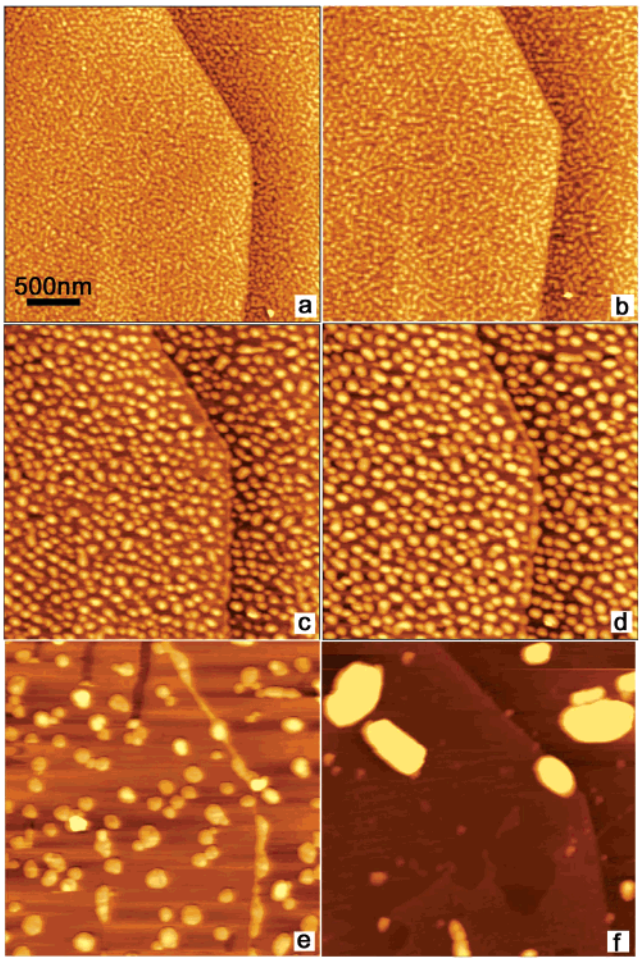

Figure 2. Evolution of local morphology for a rotaxane thin film spin-cast at room temperature and then annealed at 363 K for a time *t*: (a) t = 0 min, height range (black to white) z = 8 nm; (b) t = 2 min, z = 6 nm; (c) t = 10 min, z = 10 nm; (d) t = 15 min, z = 12 nm; (e) t = 20 min, z = 12 nm; (f) t = 90 min, z = 32 nm.

It is apparent that ξ increases linearly in time as a result of the size/distance increase of the droplets and then it saturates. In the monotonically growing regime, the increasing intensity of the peaks reflects the enhancement of spatial correlations in time. Saturation of ξ corresponds to the onset of crystallization via a massive ripening and disappearance of the droplets in the surroundings of the growing crystallite. The corresponding $g(r)$ shows an abrupt decrease of the intensity of the peaks, as the mosaic of droplets disappears in favor of the crystallites' growth.

In Figure 4, the processes of nucleation and crystallization via depletion/incorporation of the droplets from the area surrounding the nucleus are shown.

The growing crystal exhibits the following features: (i) it nucleates 3D since the early stages, as apparent from the profile (Figure 4f) where the lowest layer is 5−6 nm high; (ii) edges and corners become sharper and better defined in time; (iii) the crystal exhibits a layered structure with steps 1.5 ± 0.3 nm high. This value is consistent with the interlayer spacing along the *b* direction reported for rotaxane **1** crystal (1.39 nm).[15]

Texturing Analysis by AFM. As crystallization is completed, droplets have completely disappeared and a texture of crystallites on the graphite surface is formed, as shown in Figure 5. The angular distribution of the fast growth directions of the **1** crystal with respect to the underlying graphite lattice was measured

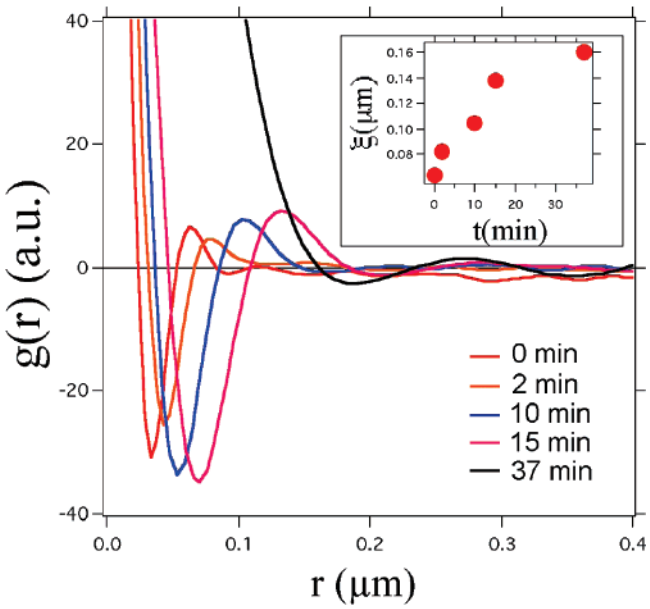

Figure 3. Evolution of the height−height correlation function extracted from the AFM images in Figure 2, showing both the increase and the shift in spatial correlations (height and position of the first maximum). Inset shows the evolution of the correlation length, viz. the position of the first maximum.

by performing 2D-Fast Fourier Transform (FFT) on AFM images. From the 2D-FFT (inset in Figure 5) it appears that the main alignment directions of the rotaxane **1** crystals form roughly 120° angles among themselves. An estimate for the angular spread in the three directions from the 2D-FFT comes out to about 10°, so the angles between the directions of in-plane orientation of **1** crystals are 120° ± 10°. The average domain size in HOPG substrate used (grade Z) is ∼5−10 μm, which matches the typical AFM image size as in Figure 5. Mosaicity of HOPG used is 3.5 ± 1.5°, which sets the lower intrinsic limit on the spread of the angular distribution of **1** crystal on HOPG. The larger spread, viz. 10°, then largely arises from the finite width of the rotaxane crystals.

The underlying graphite substrate orients the growth of the rotaxane crystallites. The texturing is largely the result of the preferential nucleation of the crystallites and the larger molecular diffusivity along terraces and steps of HOPG. Whether epitaxy, in terms of commensuration between rotaxane and graphite lattices, is relevant will be addressed in the following subsection.

Structural Investigation by TEM and SAED. The annealed samples were transferred from the graphite substrate to a copper grid coated with amorphous carbon or were prepared directly by casting and annealing on amorphous carbon thin films for TEM investigations. Figure 6a shows a bright field image of **1** deposited on isotropic amorphous carbon. Large lamellae coexist together with less defined droplets, which are largely interconnected. Large area bright field TEM images show the same type of morphologies as the ones observed with AFM. Upon closer examination, it appears that these smaller objects show straight edges and indeed bear similarity to the larger lamellar crystals. One should also note that it is possible to identify large domains where neighboring objects share a common in-plane orientation. Moreover, at an initial stage of the coalescence of droplets, a pre-transitional state is observed, with droplets assuming shapes with sharp corners. The droplets give rise to a connected network which evolves into platelet crystals such

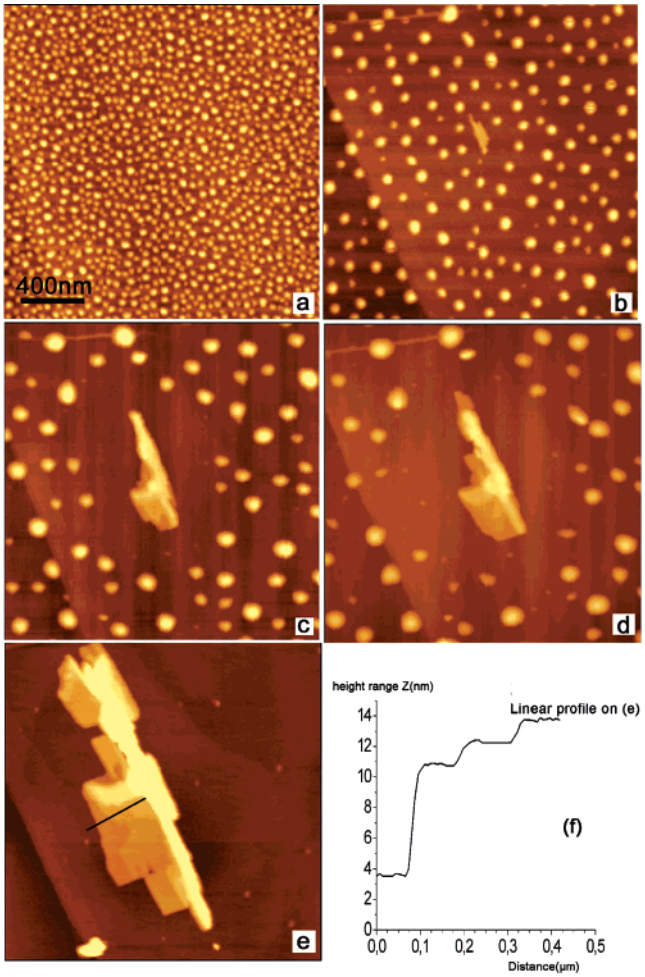

Figure 4. The rotaxane thin film is annealed at 363 K for 20 min. After formation of the first nucleus (Figure 4b), the crystal grows by capturing the smaller droplets from the surroundings. The figures show the evolution at annealing time intervals $\Delta t = 5$ min: (a) the film as spin-cast $t = 0$, height range $z = 12$ nm; (b) $t = 5$ min, $z = 18$ nm; (c) $t = 10$ min, $z = 18$ nm; (d) $t = 15$ min, $z = 19$ nm; (e) $t = 20$ min, $z = 20$ nm; (f) profile across the black line in (e).

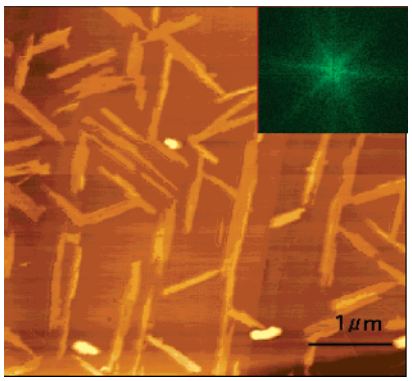

Figure 5. AFM image of **1** crystallites on HOPG showing orientation along three directions. Step edges of HOPG are also visible. Inset shows 2D-FFT of the image exhibiting a 6-fold angular symmetry.

as the one shown in Figure 6b at larger magnification. The corresponding SAED pattern is shown in Figure 6c. The indexation was assigned on the basis of the bulk crystal structure parameters of **1**.[15] The observed diffractions are of (*h*0*l*) type and therefore the contact plane of this platelet crystals with the substrate has been indexed as (010). The bounding facets corresponding to the fast growth directions are (102) and (−101). On HOPG, the crystal indexing has been done based on the structural results by TEM/SAED and comparison of the measurements from AFM images with the expected angles from the rotaxane **1** structure.

On HOPG, angles of 125°, 121°, and 59° are often observed in rotaxane crystals. These values match the 121° angle between (301) and (−101). Thus, (−101), (102), and (301) facets are found, in some cases also (−10−1) which are expected to be at 85° from (−101). From the representative AFM image of rotaxane **1** on graphite (Figure 7), we infer from the aspect ratio of the crystals that (101) and (301) are faster growing facets than (−101). The (301) facets appear pinned to the graphite steps. This suggests that graphite steps either promote nucleation of this facet, and hence the crystal grows starting from there, or they stop the growth of the (301) once it reaches the edge. This relationship between crystallographic directions of rotaxane crystals and graphite is sufficient to explain the orientation at 60° and 120° of the rotaxane crystals as in Figure 5.

Energetics of Rotaxane Surfaces. In an effort to obtain further insight into the surface properties of **1**, we performed a computational investigation of the structures and the energy of nine surfaces characterized by low values of Miller indices. In the recent past, both the short time (sub-picosecond), harmonic, and the long time (up to microsecond), large-amplitude, dynamics of this kind of systems were studied[22] with the MM3 model[23] which has become the method of choice to treat these systems. The method also reproduces rotational barriers and steric energies in cyclic and cage structures. Importantly, for the present purpose, MM3 also includes specific interatomic nonbonded potential energy functions that allow a quantitative treatment of the van der Waals and electrostatic interactions which play an essential role in hydrogen bonding and in the $\pi-\pi$ interactions between aromatic rings. Figure 8a shows the molecular orientation in the unit cell as from the crystallographic coordinates. This makes it clear that, in the lamellae, the molecules of **1** are standing with the thread almost perpendicular to the substrate. This orientation results in a contact plane made of an almost hexagonal 2D lattice of phenyl end groups edge-on on the graphite surface, as shown in Figure 8b,c. The in-plane parameters of the **1** crystal are $a = 1.057$ nm and $c = 1.075$ nm, forming an angle $\beta = 115.25°$.

The results of the geometry optimization are shown in Figure 9 and summarized in Table 1. By inspection, we notice three points about the (010) surface:

1. This surface is the second most stable of the surfaces examined. The stability vouches for (010) as a possible final product of the transformations induced by an external perturbation, this being a mechanical one either by the AFM tip or by heating in the present annealing experiment.

2. The lattice parameters of the (010) surface are within 19% misfit respectively with the lattice parameter of graphite. The

(22) (a) Leigh, D. A.; Murphy, A.; Smart, J. P.; Deleuze M. S.; Zerbetto, F. *J. Am. Chem. Soc.* **1998**, *120*, 6458−6467. (b) Deleuze, M. S.; Leigh, D. A.; Zerbetto, F. *J. Am. Chem. Soc.* **1999**, *121*, 2364−2379. (c) Bermudez, V.; Capron, N.; Gase, T.; Gatti, F. G.; Kajzar, F.; Leigh, D. A.; Zerbetto, F.; Zhang, S. W. *Nature* **2000**, *406*, 608−611. (d) Fustin, C.-A.; Leigh, D. A.; Rudolf, P.; Timpel, D.; Zerbetto, F. *Chem. Phys. Chem.* **2000**, *1*, 97−100.
(23) (a) Allinger, N. L.; Yuh, Y. H.; Lii, J.-H. *J. Am. Chem. Soc.* **1989**, *23*, 8551−8566. (b) Lii, J.-H.; Allinger, N. L. *J. Am. Chem. Soc.* **1989**, *23*, 8566−8575. (c) Lii, J.-H.; Allinger, N. L. *J. Am. Chem. Soc.* **1989**, *23*, 8576−8582.

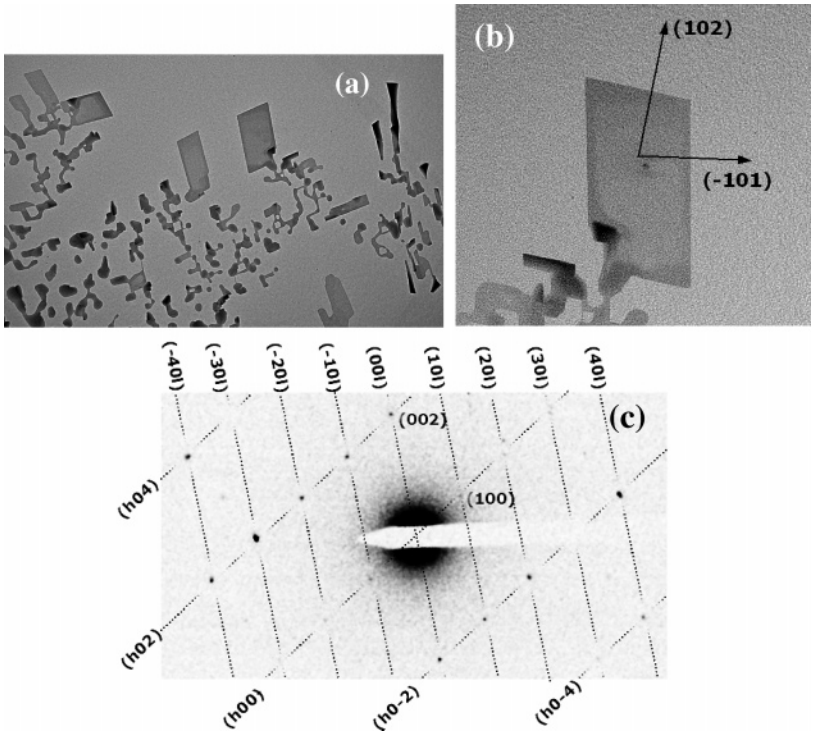

Figure 6. (a) Bright field image of annealed thin film of rotaxane **1** spin cast on amorphous carbon. (b) Larger magnification image of a single crystal of **1** grown on amorphous carbon. The facets were indexed from SAED pattern (c). (c) SAED diffraction pattern of the single crystal in (b). This set of indices leads to assigning the (010) as the basal plane of the rotaxane crystal.

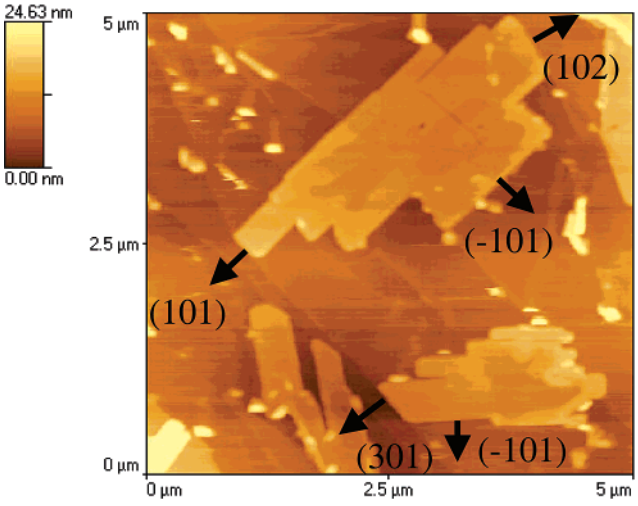

Figure 7. Indexation of rotaxane **1** crystals on HOPG.

additional role of the graphite may indeed be to further stabilize the (010) surface with respect to other minimum energy ones by epitaxy.

3. The packing of the rotaxane in the (010) surface results in some of the strongest interaction energies between either one of the two interlocked molecules (i.e., macrocycle and thread) and the surrounding environment.

When these interactions are small, one can expect that the surface is easily modified either by a scanning AFM tip or by other external stimuli such as temperature. When these interactions are large, the molecules are strongly held in place by their neighbors. Also, if this surface is formed, it therefore appears to be more difficult to disrupt compared to other surfaces.

In short, (010) appears as the best compromise for the final product of the transformation since it forfeits a small amount of surface energy, it has large interactions of ring and dumbbell with the nearby molecules, and its lattice parameters are close to those of graphite.

Table 1. Optimized Surface Energies, γ (J m^{-2}), of Rotaxane **1**[a]

surface	γ	E_{macro}	E_{thread}	SAS	SR
100	0.0516	10.83	10.97	381.07	1.29
010	0.0910	13.21	9.19	182.53	1.78
001	0.0933	14.60	13.45	375.54	1.28
011	0.1679	8.00	4.41	582.93	1.85
101	0.1799	6.49	6.34	635.19	1.56
110	0.1607	9.64	7.07	501.60	1.59
111	0.3421	4.75	3.57	673.09	1.58
012	0.1712	8.49	7.19	637.10	1.78
210	0.1408	9.76	7.49	620.53	1.71

[a] E_{macro} and E_{thread} are the sum of interactions of each of the two components of the rotaxane with the surrounding molecules. The surface accessible area, SAS (Å^2 cell^{-1}), is the size of the corrugated surface. The surface ratio, SR, is given by the SAS divided by the area of the parallelogram spawn by the lattice axes.

Discussion

The dewetting of rotaxane thin films is the first stage of a complex process leading in the steady state to the crystallization of the material. At the early stages, thermally induced dewetting is the result of either nucleation and growth of holes in some instances or a spinodal mechanism in others. The mechanism of dewetting at the early stage is presently under investigation. As the droplets are formed by either one of these paths, the following evolution is common and leads to the process described in this paper. At a later stage some droplets nucleate into crystallites and the latter grow by incorporation of the surrounding droplets until these disappear completely. The coarsening or coalescence of droplets by a mechanism like Ostwald ripening introduces the spatial correlations from the

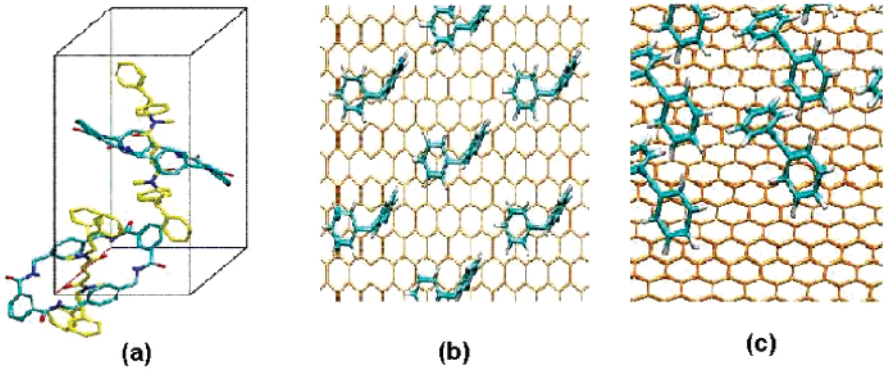

Figure 8. (a) Orientation of **1** in the unit cell; (b)−(c) contact plane of **1** on the hexagonal 2D graphite lattice.

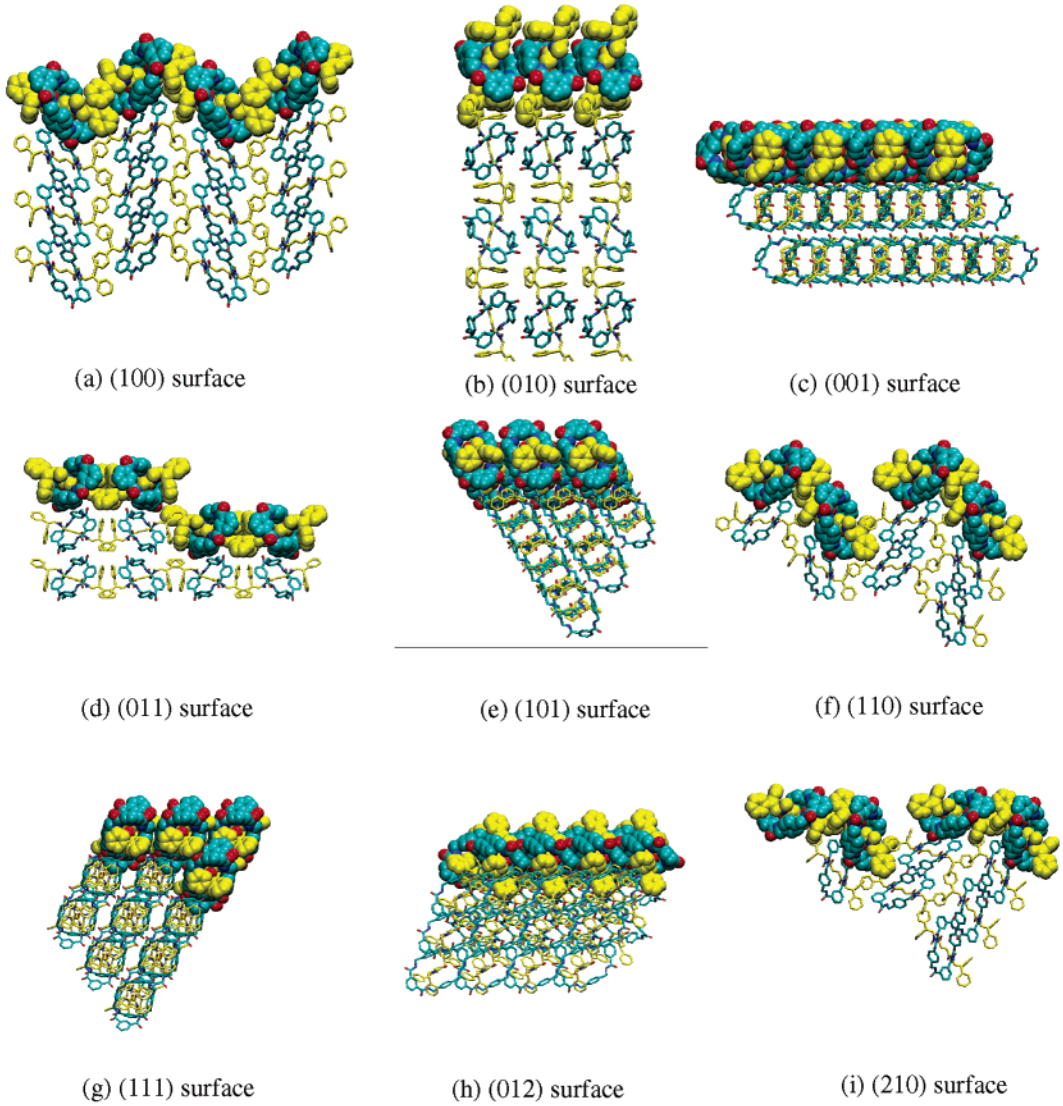

Figure 9. Optimized surface structures of **1**. The thread atoms are in yellow, while the macrocycle atoms are in blue and red.

mesoscopic to microscopic length scales. We do not know whether these droplets undergoing ripening are crystalline, polymorphic, or amorphous. At later stages, we observe that individual droplets undergo a re-structuration at the surface and possibly internally to give rise to stable nuclei. Whereas ripening is a universal phenomenon, observed in many different systems, from water to metals, polymers, colloids, and liquid crystals, the re-structuration of the individual droplets by minimum energy pathways for crystallization involves collective motion of the macrocycles with respect to the threads (this will be the subject of a forthcoming paper). The activation energy of this small amplitude motion depends on the detailed hydrogen bond motif in the rotaxanes. Therefore, the onset of crystallization is a function of the specific rotaxanes via the energy barriers for the motions in the solid state and can be controlled by design. Further discussion on the peculiarity of rotaxane architecture

with respect to the variety of molecular and supramolecular species is reported below. Because fluctuations, random or collective, have a size-dependent spectrum, we may expect lower barriers for smaller droplets. Thus, we anticipate that the time scale of nucleation of the droplets and that of coalescence may indeed cross upon thickness reduction. In this case the coalescence would involve crystalline nuclei or droplets in a pretransitional state, as also we observed.

On both amorphous carbon and HOPG we have observed that **1** crystallizes from solution mainly in the form of large lamellae having the same crystal structure as the bulk. On both substrates the contact plane of these crystals is the dense (010) plane where the terminal benzene rings (stoppers) of the thread are oriented almost normal to the surface. The lamellae have delimiting facets, which are also indexed as very dense crystal planes and the aspect ratio is in agreement with surface energy evaluation from molecular mechanics simulation. The lamellae exhibit a common orientation over large areas. On HOPG a 3-fold symmetry of the crystals orientation reveals a strong influence of the substrate on the nucleation and diffusion. The occurrence of epitaxy at the molecular scale cannot be either proven or ruled out here since our attempts to perform high-resolution STM on rotaxane ultrathin films and crystals did not provide conclusive evidence of the arrangement of the rotaxane molecules relative to the HOPG mesh. Also, we were not able to obtain diffraction patterns of the **1** crystals directly on their substrate since no sample was thin enough to enable electron transmission. The exact epitaxial conditions and the relative orientation of rotaxane crystals with respect to HOPG could thus not be determined. Nevertheless, it is worth noting that the 2D periodicity of the (001) plane of HOPG is very close to the one of the (010) contact plane of **1**. Although true 2D epitaxy is not realized, it is often observed that the matching of periodicity along a single direction is enough to lead to perfect orientation of the overgrown rotaxane layer. If epitaxy were relevant, it is worth highlighting that it does not favor the development of a new crystalline polymorph nor of a new contact plane. The bulk structure and the (010) contact plane are thus apparently the most stable ones in the conditions explored.

Conclusions

The transformation of rotaxane thin films into self-organized spatially correlated nanostructures upon a thermal perturbation has been investigated using atomic force microscopy, bright field transmission electron microscopy, selected area electron diffraction, and molecular mechanics simulations. The evolution follows a complex path, where the film first de-wets from the substrate to form nanosized droplets whose ripening gives rise to spatially correlated motives. In a later stage, the larger droplets nucleate and coalesce into crystallites that further grow into larger crystals by incorporating the surrounding droplets. Our results show that (i) the self-organized nanostructures represent a metastable state of a crystallization process, (ii) spatial correlations emerge during ripening, but they are destroyed as stable nuclei are formed and crystallization proceeds to completion, and (iii) crystallization, either on graphite or amorphous carbon films, leads to a precise basal plane, viz. (010), which has minimum surface energy. The rotaxane architecture favors the reorganization and nucleation of the film in the solid state. Low-energy trajectories leading to crystallites with stable surfaces and minimum energy contact plane are found to occur via concerted, small amplitude, internal motions without disruption of packing and intermolecular contacts.

These features combine to make rotaxanes an extremely interesting system for the investigation of self-organization across length scales, and therefore for devising new patterning strategies based on the control of spontaneous length scales.

Acknowledgment. We are grateful to Martin Brinkmann, Marc Schmutz, and Bernard Lotz for kindly providing access to the TEM facility of CNRS-Institut Charles Sadron Strasbourg, and for useful discussions. This work is partially supported by RTN Project EMMMA. R.K. acknowledges ICTP for TRIL fellowship.

Supporting Information Available: Information about materials and thin films, characterization by TEM/SAED/AFM, and MM3 calculations regarding the crystal surface energies of **1**; the complete references for 5d, 7d, 7f, and 7h. This material is available free of charge via the Internet at http://pubs.acs.org. See any current masthead page for ordering information and Web access instructions.

JA054886O